Check for updates

Comparative Studies on Two-Dimensional (2D) Rectangular and Hexagonal Molybdenum Dioxide Nanosheets with Different Thickness

Nasrullah Wazir[1], Chunjie Ding[1], Xianshuang Wang[1], Xin Ye[1], Xie Lingling[1], Tianqi Lu[1], Li Wei[1], Bingsuo Zou[1,2]* and Ruibin Liu[1]*

Abstract

Molybdenum dioxide (MoO_2) a kind of semi-metal material shows many unique properties, such as high melting point, good thermal stability, large surface area-to-volume ratio, high-density surface unsaturated atoms, and excellent conductivity. There is a strong connection between structural type and optoelectronic properties of 2D nanosheet. Herein, the rectangular and hexagonal types of thin and thick MoO_2 2D nanosheets were successfully prepared from MoO_3 powder using two-zone chemical vapor deposition (CVD) with changing the experimental parameters, and these fabricated nanosheets displayed different colors under bright-field microscope, possess margins and smooth surface. The thickness of the blue hexagonal and rectangular MoO_2 nanosheets are ~ 25 nm and ~ 30 nm, respectively, while typical thickness of orange-colored nanosheet is around ~ 100 nm. Comparative analysis and investigations were carried out, and mix-crystal phases were indentified in thick MoO_2 as main matrix through Raman spectroscopy. For the first time, the emission bands obtained in thick MoO_2 nanosheets via a Cathodoluminescence (CL) system exhibiting special properties of semi-metallic and semi-conductors; however, no CL emission detected in case of thin nanosheets. The electrical properties of thin MoO_2 nanosheets with different morphologies were compared, and both of them demonstrated varying metallic properties. The resistance of thin rectangular nanosheet was ~ 25 Ω at ± 0.05 V while 64 Ω at ± 0.05 V was reported for hexagonal nanosheet, and observed lesser resistance by rectangular nanosheet than hexagonal nanosheet.

Keywords: Molybdenum dioxide nanosheets, Hexagonal, Rectangular, Chemical vapor deposition (CVD)

Introduction

To date, various 2D materials have been synthesized such as graphene, transition metal dichalcogenides, antimony, black phosphorus, Mo_2C, and h-BN [1–6]; illustrate incredible potential for new type of optoelectronic devices owing to their unique properties and rich in feasibility for the fabrication of 2D materials technologies [7]. Certainly, some of specific 2D materials have shortcomings such as zero band gap, low absorption efficiency, and instability in open atmosphere are the challenges in fabrication of ideal nanoscale devices. In order to overcome these challenges, the transition metal oxides (TMOs) have been found effective 2D materials in terms of possessing high conductivity, piezoelectricity, colossal magnetoresistance, better stability in open environment and superconductivity, etc. [8–10]. Molybdenum dioxide is a typical TMOs material having three crystalline polymorphic forms; hexagonal phase ($P6_3/mmc$) [11], tetragonal phase ($P4_2/mnm$) [12] and monoclinic ($P2_1/c$) [13], and also possesses a partially rutile configuration [14] containing MoO_6,

* Correspondence: zoubs@bit.edu.cn; zoubs@gxu.edu.cn;
liuruibin8@gmail.com
[1]Beijing Key Lab of Nanophotonics and Ultrafine Optoelectronic Systems, School of Physics, Beijing Institute of Technology, Beijing 100081, People's Republic of China
Full list of author information is available at the end of the article

octahedrally linked Mo through oxygen atoms in the edges of unit cell involves four MoO_2 units opposite to two unit cells [15, 16]. It is well known that the properties of molybdenum oxides are strongly dependent on their crystalline structures; in particular, the rutile structure of MoO_2 is interesting due to possession of superb metallic-like electrical conductivity [12], low electrical resistivity, high melting point [17, 18], facile ion transport [19], and excellent chemical stability [20]. It has been interrelated to various interatomic bondings and comparatively over the top density of states at the Fermi level. The presence of free electrons generate Mo^{4+} in MoO_2 in contrast to generation of Mo^{6+} from MoO_3; hence, all the valence electrons in molybdenum metal are covalently bonded to nearest oxygen atoms [21, 22]. A small variation in Mo valence may cause significant fluctuations in physical properties of the molybdenum oxides. For instance, it is possible to obtain compounds of other oxides with diverse physical properties [23, 24].

Therefore, the crystallinity, shape, and size of product can be achieved smoothly by changing various parameters under desired synthesis techniques; for example, Spevack et al. obtained monoclinic structure MoO_2 ($P2_1/c$) from α-MoO_3 by thermal reduction method [25]. Alves et al. reported the electronic and structural transitions at various temperature and resulted in increasing thermal expansion, heat capacity, and electrical resistivity of single-crystal MoO_2 [26]. Jacob et al. described the deformation in MoO_2 at high temperature and acknowledged a phase transition occurring at specific temperature with transformation of distorted rutile structure ($P2_1/c$) into a hexagonal rutile structure ($P4_2/mnm$) [27]. In addition, the electronic structure and properties of molybdenum oxide materials vary with thickness [16], and MoO_2 nanostructures have been widely used in electro-chemical supercapacitors [28], catalysis [18], sensing [29], energy storage [30], electrochromic displays [31], and energy conversion regimes [32] because of their superior charge transport properties [24]. Furthermore, various methods have been used for synthesis of diverse morphologies MoO_2 for achievement of exceptional properties. MoO_2 has no van der Waals crystalline property and hence, cannot be exfoliated to layers from bulk. Mostly, MoO_2 has been synthesized from their precursors by different techniques such that hydrothermal and solvothermal routes [11], thermal decomposition of molybdates [33], solid reduction reaction [34], and electrospinning [35] having varied morphologies, such as nanoparticles [36], nanowires [31], nanorods [28], nanostars [28], nanosheets [37], hollow [38], and mesoporous particles [39]. However, these methodologies are found ineffective to control the surface morphology and size of particles [22].

Two-dimensional MoO_2 nanosheets with thin and well homogenous surface morphology have been considered suitable for high metallic conductivity, perfect chemical

stability, and enable 2D MoO_2 nanosheets as promising for integration of 2D materials in a variety of electronic structures and nanoscale devices [40]. Here, we have presented a comparative study and synthesis of two-dimensional (2D) rectangular and hexagonal molybdenum oxide nanosheets supported on SiO_2/Si without post-annealing treatment via CVD technique: the two types of ultrathin MoO_2 nanosheets with various thickness were successfully prepared and characterized by Raman, AFM, and CL, as well as I–V characterizations. The electrical behavior of the molybdenum oxides varies from semi-metal to wide bandgap semi-conductor as it depends on thickness and oxides state. The time adjustment controls the deposition, thickness, and determines the sub-oxide states [41]. Insight into the oxides' phase stability, ranges, and mixtures are not only significant for understanding molybdenum oxide nanosheets, but also important for other TMOs for optoelectronic applications [42].

Methods/Experimental Section
Synthesis of the Hexagonal MoO_2 Nanosheets
Synthesis of hexagonal molybdenum dioxides (MoO_2) nanosheets from precursor ~ 20 mg of MoO_3 powder (99.95%, Alfa Aesar) placed at one end of quartz tube in a porcelain boat and heated in two-zone furnace under nitrogen (N_2) atmosphere as shown in the Fig. 1a. The parent SiO_2/Si substrates are sequentially cleaned with deionized water, acetone, ethanol, and isopropanol through sonication and arranged the clean substrates at 3 cm distance from precursor powders. Two thermal blocks were placed at the end of the quartz tube; before heating, the quartz tube was purged with a N_2 (99.999%) at a constant gas flow rate of 200 sccm for 20 min to remove O_2 and other contaminants and then reduced flow rate to 20 sccm as a carrier gas. The left heating zone was set up to 480 °C at rate of 10 °C min^{-1} rise in temperature, while the right zone was set up to 780 °C at the same rate of rising temperature, and held for 20 min in the presence of N_2 environment. After the
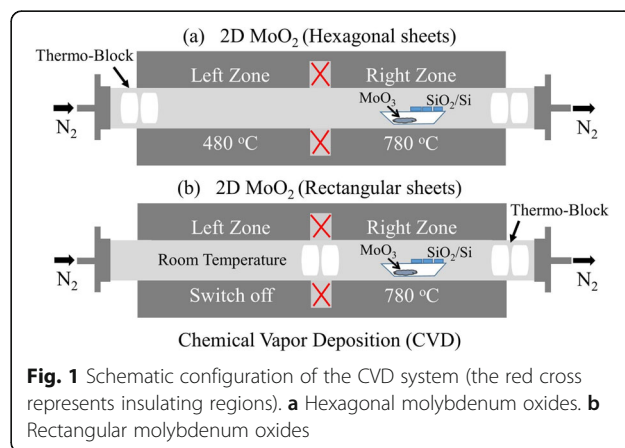

Fig. 1 Schematic configuration of the CVD system (the red cross represents insulating regions). **a** Hexagonal molybdenum oxides. **b** Rectangular molybdenum oxides

completion of reaction, the furnace was left to naturally cool down to room temperature and finally obtain hexagonal MoO_2 nanosheets deposited on the SiO_2/Si substrates.

Synthesis of the Rectangle MoO_2 Nanosheets

In similar fashion mentioned above, the rectangle molybdenum dioxide (MoO_2) nanosheets were grown in two-zone tube furnace under N_2 atmosphere, as shown in the Fig. 1b. In this set up, the thermo-blocks were placed close to the middle of the tube: left zone was set at room temperature and the rest of the parameters were remained the same, as were set for the synthesis of hexagonal MoO_2 nanosheets, to grow rectangular MoO_2 nanosheets on the SiO_2/Si substrates.
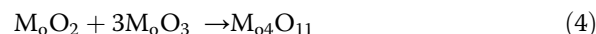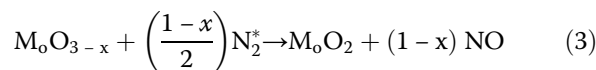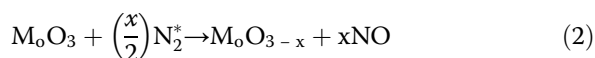
Fabrication of the Devices

E-beam lithography was followed for fabrication of electrodes with Ti (10 nm)/Au (90 nm) for hexagonal and the rectangular MoO_2 nanosheets as contact.

Characterizations

AFM images were obtained using atomic force microscope, a Dimension Edge PSS (Bruker, Inc., Karlsruhe, Germany) in a non-contact mode. SEM images were recorded under a Hitachi S-4800 microscope working at 10.0 kV. Optical photographs were recorded by an optical microscope (Olympus BX51M). Raman spectra was acquired by a confocal Raman setup (based on spectrometer Princeton Acton SP2500). Cathodoluminescence (CL) spectra was captured by a CL measurement setup (Horiba Is-100-em-type2). I–V curves of the devices were measured by a micro probe station system (Keithley 4200-SCS).
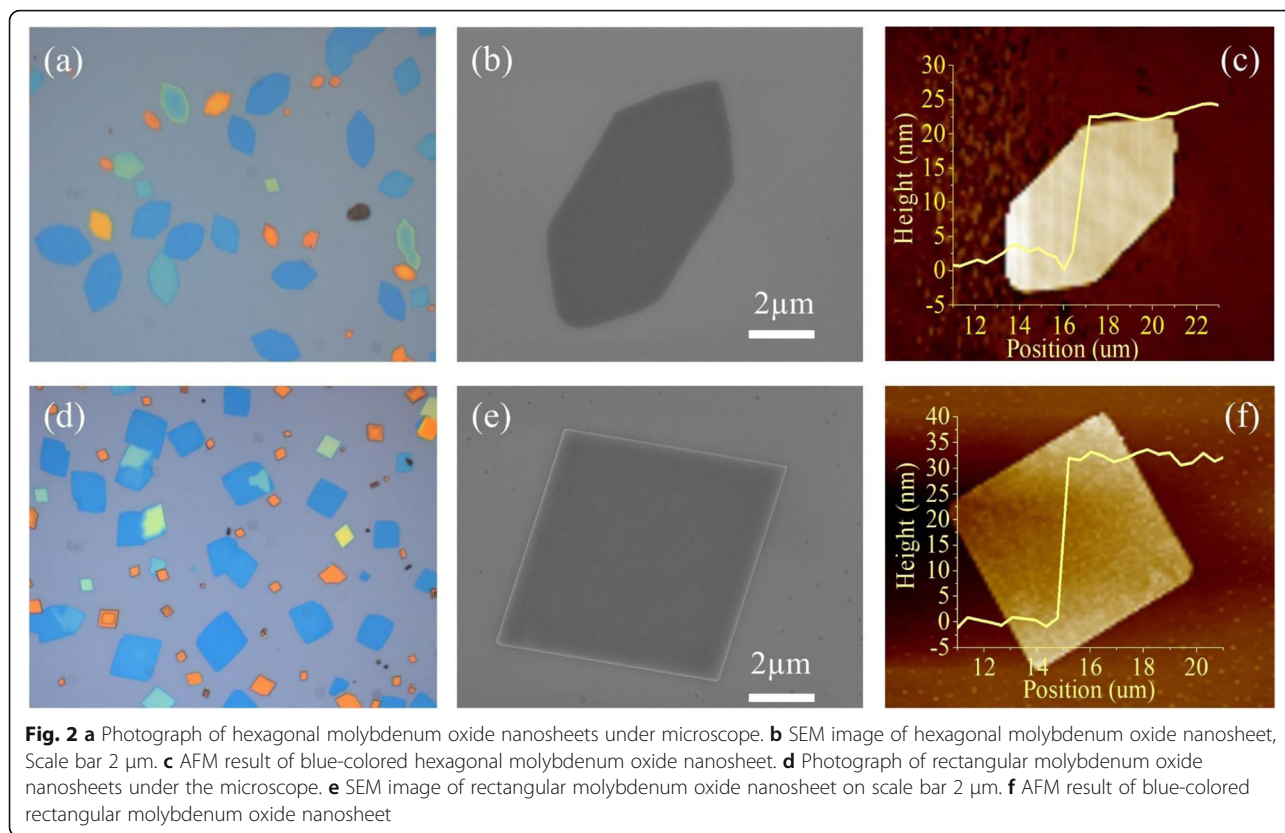
Results and Discussions

Different conditions were set for synthesis of rectangular and hexagonal TMO's nanosheets, and the changing parameters resulted in different shaped nanosheets as shown in Fig. 1. The literature suggests some possible reaction mechanism for CVD-grown nanosheets; some of nitrogen gas molecules are converted into ionized nitrogen molecules at specific temperature by thermal irradiation in a tube furnace, and such ionized nitrogen molecules are marked by N_2^* [43]. At the desired temperature, the molecules of MoO_3 collide with the ionized N_2^* molecules, which produce a series of possible reactions in the presence of inert nitrogen gas environment [44–46].
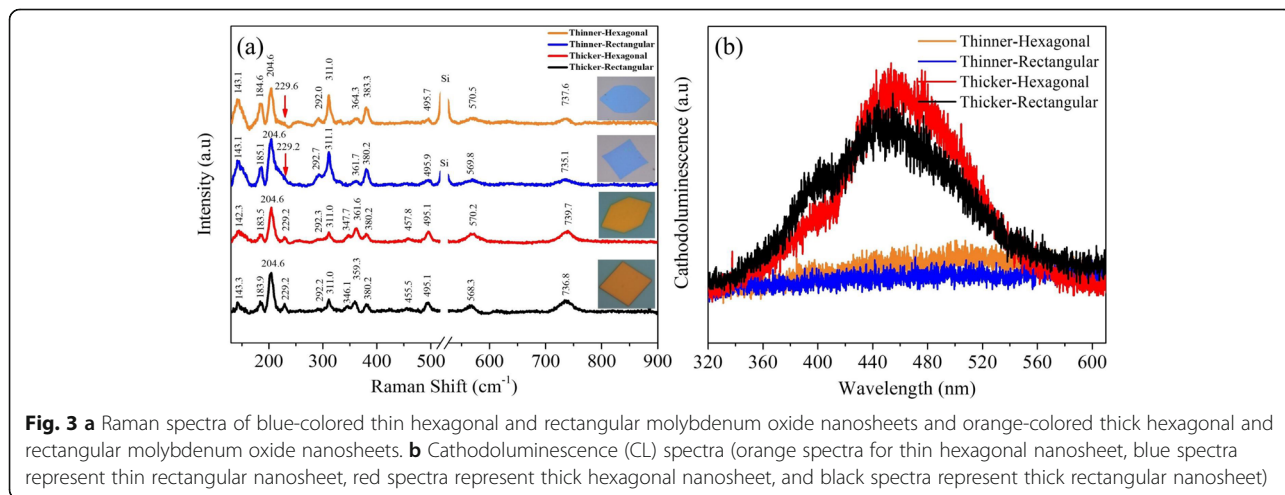
$$e + N_2 \rightarrow N_2^* + e \qquad (1)$$

$$M_oO_3 + \left(\frac{x}{2}\right)N_2^* \rightarrow M_oO_{3-x} + xNO \qquad (2)$$

$$M_oO_{3-x} + \left(\frac{1-x}{2}\right)N_2^* \rightarrow M_oO_2 + (1-x)\,NO \qquad (3)$$

$$M_oO_2 + 3M_oO_3 \rightarrow M_{o4}O_{11} \qquad (4)$$

The structure of evaporated MoO_3 molecules may change to different kinds of morphologies nanosheets, either by increasing or decreasing N_2 gas flow and the holding time at desired temperatures [45]. During the diffuse of molecules toward substrates, they start aggregation to form different kinds of regular rectangular and hexagonal MoO_2 sheets.

Figure 2a shows CVD fabricated hexagonal MoO_2 nanosheets far better than the solution-based synthesis of hexagonal MoO_2 nanosheets [47, 48]. Furthermore, different phase structures of rectangular MoO_2 can be obtained using CVD technique with certain control parameters; the temperature of heating zones, location of thermal blocks, and position of substrates as shown in Fig. 2d. Fixing the temperature of left heating zone at 480 °C was extremely important for synthesis of hexagonal MoO_2 nanosheets. The basic mechanism of hexagonal MoO_2 nanosheets is a temperature gradient. Xu, X., et al. report high dependency of morphologic variation is thermodynamics and kinetics influence in crystal growth process, which is based on the difference in thermodynamic stability and the lattice strain between the phases [49]. Both low- and high-temperature zones play crucial role in fabrication of hexagonal nanosheets; however, the variation in temperature of high-temperature zone is very effective for growth of rectangular MoO_2 nanosheet. In addition, Wang, S., et al. reported an evolution of two-dimensional nanosheets that are highly dependent upon the spatial location of the substrates [50]. Yang, X., et al. also reported the temperature-dependent growth of regular nanosheets morphology and further explained the chemical vapor mechanism with the help of first principle KMC method [51]. There are some blue- and orange-colored hexagonal and rectangular nanosheets of different thickness; blue-colored nanosheets are thinner than orange-colored nanosheets and are in close agreement with characteristics of other 2D materials [52]. Mixed colors mean a layered nanosheet formed various thicknesses, as shown in Fig. S1 and Fig. S2 in supplementary information. The thickness of the nanosheets monotonically decreased in sequence: orange color, yellow color, and blue color, which depends on the variation of synthetic parameters. Figure 2b, e shows the amplified SEM image of the typical hexagonal and rectangular nanosheet, illustrating smooth surface, clear margins, regular shape of high quality, and 10 μm in length. The AFM measured the blue hexagonal and rectangular nanosheets as ~ 25 nm and ~ 30 nm thick, respectively, as shown in the Fig. 2c, f.

Fig. 2 a Photograph of hexagonal molybdenum oxide nanosheets under microscope. **b** SEM image of hexagonal molybdenum oxide nanosheet, Scale bar 2 μm. **c** AFM result of blue-colored hexagonal molybdenum oxide nanosheet. **d** Photograph of rectangular molybdenum oxide nanosheets under the microscope. **e** SEM image of rectangular molybdenum oxide nanosheet on scale bar 2 μm. **f** AFM result of blue-colored rectangular molybdenum oxide nanosheet

Raman spectra was acquired to investigate the quality and uniformity of as-grown MoO_2 nanosheets. Here, we present Raman spectra of rectangular and hexagonal MoO_2 nanosheets having different colors under the irradiation of 532 nm laser. In Fig. 3a, the Raman peaks obtained from thin hexagonal nanosheet (blue color) locate at 143.1, 184.6, 204.6, 229.6, 292.0, 311.0, 364.3, 383.3, 495.7, 570.5, and 737.6 cm^{-1}, respectively. In comparison to the thin rectangular nanosheet, blue color peaks are consistent with a little peak shift at 143.1,

185.1, 204.6, 229.2, 292.7, 311.1, 361.7, 380.2, 495.9, 569.8, and 735.1 cm^{-1}, respectively. Both types of thin blue-colored nanosheets got the same numbers of Raman peaks; however, an additional strong silicon's peak was obtained at 526 cm^{-1} in blue-colored hexagonal nanosheet. In fact, the peak shift originates from the difference in thickness of nanosheets; hexagonal nanosheets are thinner than rectangular nanosheets, as shown in Fig. 2c, f. The additional peak location for silicon happened from laser penetration, hitting silicon surface,

Fig. 3 a Raman spectra of blue-colored thin hexagonal and rectangular molybdenum oxide nanosheets and orange-colored thick hexagonal and rectangular molybdenum oxide nanosheets. **b** Cathodoluminescence (CL) spectra (orange spectra for thin hexagonal nanosheet, blue spectra represent thin rectangular nanosheet, red spectra represent thick hexagonal nanosheet, and black spectra represent thick rectangular nanosheet)

served as substrate, and attributed to blue-colored hexagonal and rectangular nanosheets' thickness compared to orange-colored thick hexagonal and rectangular nanosheets, as shown in Fig. 3a. For thick hexagonal nanosheets, 13 peaks were obtained with the peak position at 142.3, 183.5, 204.6, 229.2, 292.3, 311.0, 347.7, 361.6, 380.2, 457.8, 495.1, 570.2, and 739.7 cm^{-1}, respectively. The 13 peaks noted for thick rectangular nanosheet at position of 143.3, 183.9, 204.6, 229.2, 292.2, 311.0, 346.1, 359.3, 380.2, 455.5, 495.1, 568.3, and 736.8 cm^{-1} having small variation in position compared to hexagonal nanosheets. The thickness induced few additional peaks at different wavenumber as compared to the blue-colored thinner nanosheets [53]. The identification details of Raman peaks for thin/thick hexagonal and rectangular nanosheets are given in Fig. S3 in supplementary file; the results are well agreed with the reported results of monoclinic MoO_2 thin film fabricated by different CVD synthesis routes [54, 55]: thickness and peaks shifting depend on growth's conditions [56, 57]. In the present work, for the first time, we report 13 vibrational peaks for orange color, while 11 peaks for blue-colored regular hexagonal and rectangular MoO_2 nanosheets, confirming the existence of mixed structures in MoO_2 nanosheets. The sharp and strong peaks confirmed better crystallinity compared to other reported results [15, 54, 55].

We can conclude from these four typical nanosheets that all of them contain a complex and mix structures, such as pure MoO_3, MoO_{3-x}, monoclinic MoO_2, orthorhombic MoO_3 (α-MoO_3), and orthorhombic Mo_4O_{11}. The Raman peak at 289 cm^{-1} is assigned to pure MoO_3, 142 cm^{-1} to MoO_{3-x} [58] and the peak at 287 cm^{-1} is associated with orthorhombic α-MoO_3 [59]. Dieterle, M. reported Raman peaks for different molybdenum oxides; orthorhombic MoO_3, monoclinic MoO_2, and orthorhombic Mo_4O_{11}; the bands at 290–292 cm^{-1} are considered to be raised from orthorhombic MoO_3 (α-MoO_3), while Raman peaks at 183, 306 cm^{-1} raised from orthorhombic Mo_4O_{11} [60]. The peaks at 380 cm^{-1} were assigned to MoO_2 [61], and 460 cm^{-1} to α-MoO_3 [62]. The Raman spectra results of our synthesized nanosheets are presented in Fig. 3a. Raman spectra results of individual nanosheets are available in supplementary Fig. S3. Therefore, the Raman peaks in our results are associated with different structural phases of various molybdenum oxides: 142.3 ~ 143.3 cm^{-1} (MoO_{3-x}), 183.5 ~ 185.1 cm^{-1} (Mo_4O_{11}), and 204.6 cm^{-1} (MoO_2). Moreover, peaks at 229.2 ~ 229.6 cm^{-1} (MoO_2) present in orange-colored nanosheets are sharper and broader compared to blue-colored nanosheets, which confirm existence of multiple strains in thick nanosheets. The peaks at 292.0 ~ 292.7 cm^{-1} (α-MoO_3) in blue-colored nanosheets are sharper and broader than orange-colored

nanosheets. The peaks at 311.0 ~ 311.1 cm^{-1} (Mo_4O_{11}) exist in all four types of nanosheets; the more intense peak is in thin blue-colored nanosheets compare to orange-colored nanosheets. However, the peaks at 346.1 ~ 347.7 cm^{-1} (MoO_2) only exist in orange-colored nanosheets. Mostly, all these peaks are present in all kinds of nanosheets with little variation; peaks at 359.3 ~ 364.3 cm^{-1} for (MoO_2) and peaks at 380.2 ~ 383.3 cm^{-1} (MoO_2) were present in all nanosheets; however, the peaks at 455.5 ~ 457.8 cm^{-1} (α-MoO_3) are only present in orange-colored nanosheets. Major peaks are well matched with molybdenum dioxides and raised in all nanosheets, e.g., peaks at 495.1 ~ 495.9 cm^{-1} (MoO_2), 568.3 ~ 570.5 cm^{-1} (MoO_2) and 735.1 ~ 739.7 cm^{-1} (MoO_2). The sub-oxides happened due to inter valence transitions; in sub-oxides, the distance between Mo atoms are associated with oxygen atoms, in which laterally tetrahedral *c* axis increased with increasing distortion of the bond from undisturbed portion to shear plane. This affects the completely polarized modes parallel to *c* axis: the polarized modes perpendicular to *c* axis are affected by the distances of M=O bond. The escaping of oxygen atoms from pure MoO_3 after treatment with high temperature confirmed shear crystallographic structures via prolonged shear defects, finishing the translational symmetry [58]. The larger numbers of extra peaks are noted for orange-colored hexagonal and rectangular nanosheets other than the regular peaks of molybdenum dioxides; the peaks at 142.3 ~ 143.3 cm^{-1} for MoO_{3-x}, the peaks at 292.2 ~ 292.3, and 455.5 ~ 457.8 cm^{-1} for α-MoO_3, and peaks at 183.5 ~ 183.9 and ~ 311.0 cm^{-1} for Mo_4O_{11}.
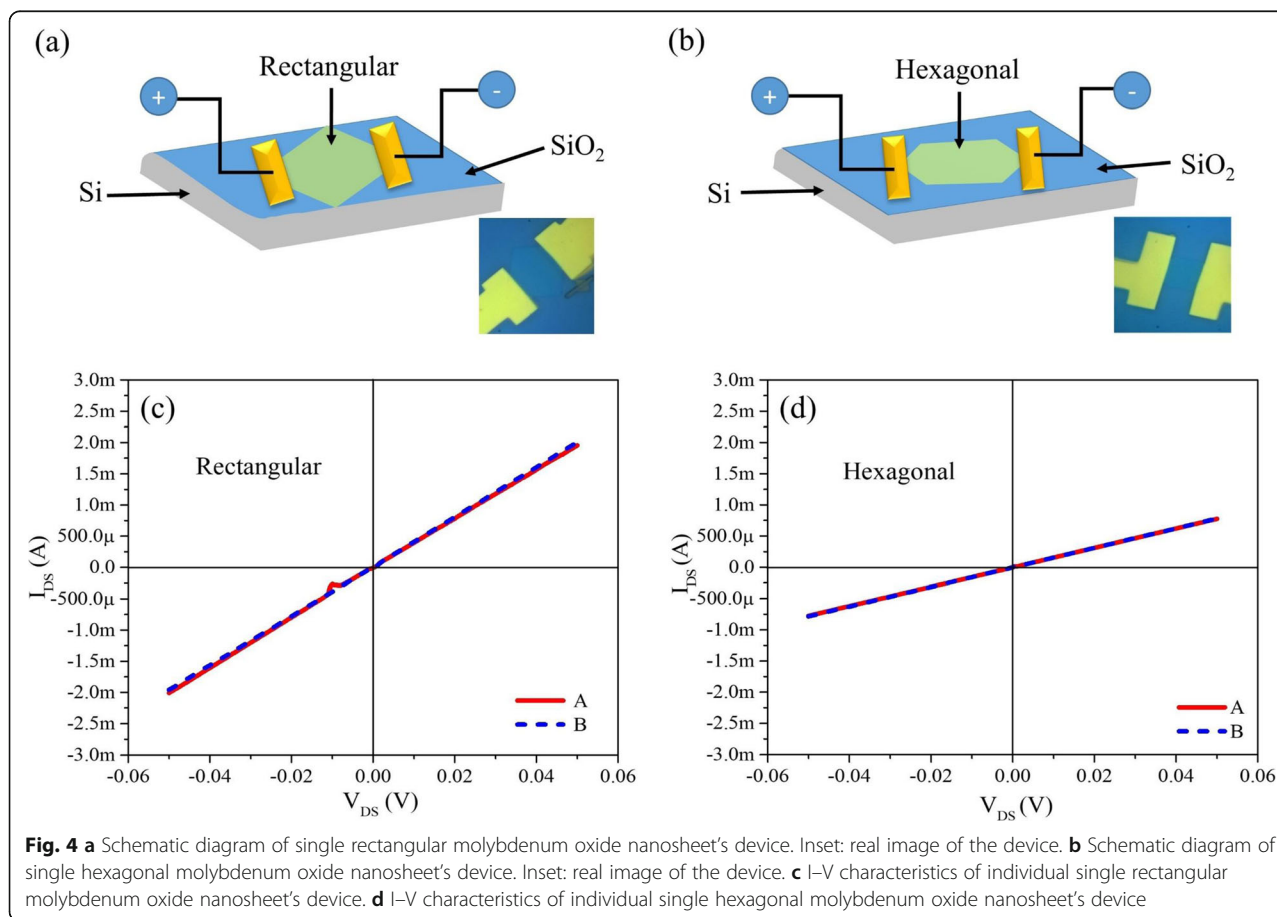
For further verification, the Cathodoluminescence (CL) is carried out to verify the structural phase's impact of complex molybdenum oxide structural phases on the metallic properties of both thick hexagonal and rectangular nanosheets. Theoretically, the semi-metallic MoO_2 will partially transform into semi-conductor due to involvement of MoO_3. However, it is very difficult to measure the PL spectrum of pure MoO_2 nanostructures due to the metallic characteristics: MoO_3 is a wide bandgap semi-conductor with a weak luminescent intensity until conversion and disappearance of MoO_3 to MoO_{3-x}, and further conversion to MoO_2 nanosheets [63]. Hence, no luminescent spectrum reported for hexagonal and rectangular molybdenum oxide nanosheets.

The Cathodoluminescence (CL) properties of molybdenum thick nanosheets revealed the electronic transition between the conduction and valence bands due to the presence of suboxides. As shown in the Fig. 3b, the CL spectra acquired for thick hexagonal and rectangular molybdenum oxide nanosheets show a small CL peaks at 410 nm (3.02 eV), while a stronger and wider peaks at 454 nm (2.73 eV) generated from nanosheets. The

weaker peaks at 410 nm in both CL spectra are similar to MoO_3 spectra, and the weak emission may be associated with a trap state recombination: 454 nm band assigned to defect-related trap-states originated from oxygen vacancies [64]. The emitted photon energy for pure MoO_3 located at 3.02 eV instead of 3.2 eV for bandgap indicates the conversion of MoO_3 powder into MoO_{3-x} and was verified via Raman spectra results. The broadband CL spectra that vary from 3.02 to 2.73 eV confirmed the mixed nanostructures in thick nanosheets, possessing metal-semi-conductor gradient behaviors. These molybdenum oxides are related to the development of carrier concentrations, oxygen vacancy concentrations in reduced MoO_3, and free-electron concentration in MoO_2. These studies advanced the knowledge of structural and optical properties of sub-stoichiometric molybdenum oxide nanosheets, contributing to the development of advanced optical devices. Similar CL spectra are reported for other transition metal oxides, such as WO_3 and α-Fe_2O_3 [65]. The CL spectra detection issue in thin nanosheets is described and reported in literature. The CL intensity of the flakes decreased with the decrease in layer thickness; thin-layered flakes are transparent to electron beam; created electron-holes are directly proportional to their thickness [66].

Bourrellier, R., et al. verified broadband luminescence detection in low-quality crystals, which is not related with extrinsic defects, but obviously with intrinsic defects that can be generated by electron irradiation [67]. Recently, Zhou, N., et al. reported strong CL intensity orientation from increasing of defect concentration and increasing flake thickness, but the intensity of CL emission decreased with the decrease of flake thickness [68]. In spite of this effect, the thick flakes show a significant luminescence in comparison to the thin flakes. This is the reason that CL spectra of pure thin MoO_2 cannot be detected in thin nanosheets; the CL spectra of both thin hexagonal (orange-colored spectra) and rectangular nanosheet (blue-colored spectra) are presented in Fig. 3b.

The thin hexagonal and rectangular nanosheets possess metallic characteristics confirmed by I–V measurement, as shown in Fig. 4 and supporting information (SI) in Fig. S4. We have fabricated two terminals containing six devices on blue-colored thin nanosheets and measured I–V curves with same parameters; three of them were rectangular nanosheets, and the rest of the three were hexagonal nanosheets, as shown in the inset of Fig. 4a, b, respectively. The contacts were fabricated with Ti/Au as electrodes. The schematic diagram of single rectangular and hexagonal molybdenum oxide

Fig. 4 a Schematic diagram of single rectangular molybdenum oxide nanosheet's device. Inset: real image of the device. b Schematic diagram of single hexagonal molybdenum oxide nanosheet's device. Inset: real image of the device. c I–V characteristics of individual single rectangular molybdenum oxide nanosheet's device. d I–V characteristics of individual single hexagonal molybdenum oxide nanosheet's device

nanosheets' devices are shown in Fig. 4a, b. In Fig. 4c, d, the I–V curves of both types of nanosheets are measured by sweeping the bias voltage from negative (– 0.05 V) to positive (+ 0.05 V) for several times without show any variation in devices and displayed linear behavior with Ohmic contact between the nanosheets and electrodes of devices. Ohmic equation was utilized for resistance measurement, $R = V/I$, where R represents resistance, V voltage, and I current; resistance of rectangular and hexagonal nanosheets were measured $\sim 25\ \Omega$ at ± 0.05 V and 64 Ω at ± 0.05 V, respectively, which further confirmed that rectangular nanosheet has less resistance than hexagonal nanosheet.

Additionally, the resistance (R) of blue-colored thin rectangular nanosheets are $\sim 30\ \Omega$ at ± 0.05 V and ~ 43 Ω at ± 0.05 V as shown in Fig. S4a, b in supporting information (SI); however, resistance (R) of blue-colored thin hexagonal nanosheets are $\sim 61\ \Omega$ at ± 0.05 V and $\sim 61\ \Omega$ at ± 0.05 V as shown in Fig. S4c, d. This verifies that the blue-colored thin rectangular nanosheets have lesser resistance at the same parameters than blue-colored thin hexagonal nanosheets.

Conclusions

In this work, we report the control-synthesis of rectangular and hexagonal molybdenum oxide nanosheets from single precursor powdered MoO_3 without post-annealing treatment through CVD methods. Comparative analysis and investigations were carried out using different spectroscopic techniques: Raman spectra, optical photograph, scanning electron microscopy, atomic force microscopy, and Cathodoluminescence (CL). The optical contrast depends on the thickness of nanosheets. SEM results confirmed well-symmetry and smooth morphology of controlled nanosheets. AFM analysis measured ~ 30 nm thickness of thin rectangular nanosheets, and ~ 25 nm hexagonal nanosheet. Raman spectra results reveal existence of mixed structures in MoO_2 nanosheets due to the complex crystalline structures. Strong spectral response and peaks shifting depends on thickness of nanosheets. Comparatively less Raman peaks were observed for thin than thicker nanosheeet, and well matched with the vibrations of crystal MoO_2 and other mixed crystals; however, some peaks disappeared in thin 2D nanosheets. The thick orange-colored nanosheets contain more peaks due to the complex structural phases of molybdenum oxide; especially, additional MoO_3 and MoO_{3-x} occurs in semi-metallic MoO_2, and thus the thick nanosheets exhibit wide bandgap semi-conductor behaviors and were further verified by Cathodoluminescence (CL) spectra. For the first time, a combined metallic and wide bandgap semi-conductor properties were observed in mixed molybdenum oxide, thick hexagonal and rectangular nanosheets. These

peaks in orange-colored nanosheets might be helpful photonic materials for practical applications in nanoscale devices; however, no CL emission is detected for thin nanosheets. The I–V curves of all devices fabricated thin rectangular or hexagonal nanosheets demonstrated linear metallic behavior due to well-established Ohmic contact between nanosheets and electrodes. The thin hexagonal nanosheet exhibited higher resistance than rectangular nanosheet. This study provides a deep comprehension of special 2D molybdenum oxide nanosheets, providing a way for modulating the properties of different types of nanosheet.

Additional Files

Additional file 1: Figure S1. The optical images reveal difference between the thickness of nanosheets associated with different colors. **Figure S2.** Optical microscopic images of nanosheets having different sizes and colors. **Figure S3.** Raman spectra of individual hexagonal and rectangular molybdenum dioxide nanosheets. **Figure S4.** The I-V curves of both blue color thin rectangular and hexagonal nanosheets devices.

Author details

[1]Beijing Key Lab of Nanophotonics and Ultrafine Optoelectronic Systems, School of Physics, Beijing Institute of Technology, Beijing 100081, People's Republic of China. [2]Guangxi Key Lab of Processing for Nonferrous Metals and Featured Materials and Key lab of new Processing Technology for Nonferrous Metals and Materials, Ministry of Education; Nano and Energy Research Center, School of Physics, Guangxi University, Nanning 530004, China.

Wazir *et al. Nanoscale Research Letters*   (2020) 15:156

Page 8 of 9

References

1. Reina A, Jia X, Ho J, Nezich D, Son H, Bulovic V, Dresselhaus MS, Kong J (2009) Large area, few-layer graphene films on arbitrary substrates by chemical vapor deposition. Nano Lett 9(1):30–35. https://doi.org/10.1021/nl801827v

2. Ji Q, Zhang Y, Zhang Y, Liu Z (2015) Chemical vapour deposition of group-VIB metal dichalcogenide monolayers: engineered substrates from amorphous to single crystalline. Chem Soc Rev 44(9):2587–2602. https://doi.org/10.1039/C4CS00258J

3. Ji J, Song X, Liu J, Yan Z, Huo C, Zhang S, Su M, Liao L, Wang W, Ni Z, Hao Y, Zeng H (2016) Two-dimensional antimonene single crystals grown by van der Waals epitaxy. Nat Commun 7:13352. https://doi.org/10.1038/ncomms13352 https://www.nature.com/articles/ncomms13352#supplementary-information

4. Li L, Yu Y, Ye GJ, Ge Q, Ou X, Wu H, Feng D, Chen XH, Zhang Y (2014) Black phosphorus field-effect transistors. Nat Nanotechnol 9:372. https://doi.org/10.1038/nnano.2014.35 https://www.nature.com/articles/nnano.2014.35#supplementary-information

5. Xu C, Wang L, Liu Z, Chen L, Guo J, Kang N, Ma X-L, Cheng H-M, Ren W (2015) Large-area high-quality 2D ultrathin Mo2C superconducting crystals. Nat Mater 14:1135. https://doi.org/10.1038/nmat4374 https://www.nature.com/articles/nmat4374#supplementary-information

6. Orofeo CM, Suzuki S, Hibino H (2014) Ultrathin chemical vapor deposition (CVD)-grown hexagonal boron nitride as a high-quality dielectric for tunneling devices on rigid and flexible substrates. J Phys Chem C 118(6):3340–3346. https://doi.org/10.1021/jp410874z

7. Fiori G, Bonaccorso F, Iannaccone G, Palacios T, Neumaier D, Seabaugh A, Banerjee SK, Colombo L (2014) Electronics based on two-dimensional materials. Nat Nanotechnol 9:768. https://doi.org/10.1038/nnano.2014.207

8. Cheng W, Baudrin E, Dunn B, Zink JI (2001) Synthesis and electrochromic properties of mesoporous tungsten oxide. J Mater Chem 11(1):92–97. https://doi.org/10.1039/B003192P

9. Lu JG, Chang P, Fan Z (2006) Quasi-one-dimensional metal oxide materials—Synthesis, properties and applications. Mater Sci Eng R Rep 52(1):49–91. https://doi.org/10.1016/j.mser.2006.04.002

10. Hirai D, Climent-Pascual E, Cava RJ (2011) Superconductivity in WO$_{2.6}$F$_{0.4}$ synthesized by reaction of WO$_3$ with teflon. Phys Rev B 84:174519

11. Yang LC, Gao QS, Zhang YH, Tang Y, Wu YP (2008) Tremella-like molybdenum dioxide consisting of nanosheets as an anode material for lithium ion battery. Electrochem Commun 10(1):118–122. https://doi.org/10.1016/j.elecom.2007.11.009

12. Shi Y, Guo B, Corr SA, Shi Q, Hu Y-S, Heier KR, Chen L, Seshadri R, Stucky GD (2009) Ordered Mesoporous Metallic MoO2 Materials with Highly Reversible Lithium Storage Capacity. Nano Lett 9(12):4215–4220. https://doi.org/10.1021/nl902423a

13. Yang LC, Gao QS, Tang Y, Wu YP, Holze R (2008) MoO2 synthesized by reduction of MoO3 with ethanol vapor as an anode material with good rate capability for the lithium ion battery. J Power Sources 179(1):357–360. https://doi.org/10.1016/j.jpowsour.2007.12.099

14. Reinhardt P, Hess BA (1994) Electronic and geometrical structure of rutile surfaces. Phys Rev B 50:12015

15. Wu H, Zhou X, Li J, Li X, Li B, Fei W, Zhou J, Yin J, Guo W (2018) Ultrathin molybdenum dioxide nanosheets as uniform and reusable surface-enhanced raman spectroscopy substrates with high sensitivity. Small 14(37):1802276. https://doi.org/10.1002/smll.201802276

16. Tokarz-Sobieraj R, Gryboś R, Witko M (2011) Electronic structure of MoO2. DFT periodic and cluster model studies. Appl Catal A Gen 391(1):137–143. https://doi.org/10.1016/j.apcata.2010.07.041

17. Sun Y, Hu X, Luo W, Huang Y (2011) Self-assembled hierarchical MoO2/graphene nanoarchitectures and their application as a high-performance anode material for lithium-ion batteries. ACS Nano 5(9):7100–7107. https://doi.org/10.1021/nn201802c

18. Yang L, Zhou W, Hou D, Zhou K, Li G, Tang Z, Li L, Chen S (2015) Porous metallic MoO2-supported MoS2 nanosheets for enhanced electrocatalytic activity in the hydrogen evolution reaction. Nanoscale 7(12):5203–5208. https://doi.org/10.1039/C4NR06754A

19. Hu B, Mai L, Chen W, Yang F (2009) From MoO3 Nanobelts to MoO2 Nanorods: Structure Transformation and Electrical Transport. ACS Nano 3(2):478–482. https://doi.org/10.1021/nn800844h

20. Zhang Q, Li X, Ma Q, Zhang Q, Bai H, Yi W, Liu J, Han J, Xi G (2017) A metallic molybdenum dioxide with high stability for surface enhanced Raman spectroscopy. Nat Commun 8(1):14903. https://doi.org/10.1038/ncomms14903

21. Katrib A, Leflaive P, Hilaire L, Maire G (1996) Molybdenum based catalysts. I. MoO2 as the active species in the reforming of hydrocarbons. Catal Lett 38(1-2):95–99. https://doi.org/10.1007/BF00806906

22. Zhu Y-P, El-Demellawi JK, Yin J, Lopatin S, Lei Y, Liu Z, Miao X, Mohammed OF, Alshareef HN Unprecedented surface plasmon modes in monoclinic MoO2 nanostructures. Adv Mater:1908392. https://doi.org/10.1002/adma.201908392

23. Akande SO, Chroneos A, Vasilopoulou M, Kennou S, Schwingenschlögl U (2016) Vacancy formation in MoO3: hybrid density functional theory and photoemission experiments. J Mater Chem C 4(40):9526–9531. https://doi.org/10.1039/C6TC02571D

24. Qin T, Wang Q, Yue D, Liu H, Zheng Y, Han Y, Gao C (2020) The effect of pressure and temperature on the structure and electrical transport properties of MoO2. J Alloys Compd 814:152336. https://doi.org/10.1016/j.jallcom.2019.152336

25. Spevack PA, McIntyre NS (1992) Thermal reduction of molybdenum trioxide. J Phys Chem 96(22):9029–9035. https://doi.org/10.1021/j100201a062

26. Alves LMS, Oliveira FS, de Lima BS, da Luz MS, Rebello A, Masunaga SH, Neumeier JJ, Giles C, Leão JB, dos Santos CAM (2017) Evidence of phase transitions in MoO2 single crystals. J Alloys Compd 705:764–768. https://doi.org/10.1016/j.jallcom.2017.02.148

27. Jacob KT, Saji VS, Gopalakrishnan J, Waseda Y (2007) Thermodynamic evidence for phase transition in MoO2–δ. J Chem Thermodyn 39(12):1539–1545. https://doi.org/10.1016/j.jct.2007.09.005

28. Zheng L, Xu Y, Jin D, Xie Y (2010) Well-aligned molybdenum oxide nanorods on metal substrates: solution-based synthesis and their electrochemical capacitor application. J Mater Chem 20(34):7135–7143. https://doi.org/10.1039/C0JM00744G

29. Liu Q, Sun C, He Q, Liu D, Khalil A, Xiang T, Wu Z, Wang J, Song L (2015) Ultrathin carbon layer coated MoO2 nanoparticles for high-performance near-infrared photothermal cancer therapy. Chem Commun 51(49):10054–10057. https://doi.org/10.1039/C5CC02016F

30. Zhu Y, Ji X, Cheng S, Chern Z-Y, Jia J, Yang L, Luo H, Yu J, Peng X, Wang J, Zhou W, Liu M (2019) Fast energy storage in two-dimensional MoO2 enabled by uniform oriented tunnels. ACS Nano 13(8):9091–9099. https://doi.org/10.1021/acsnano.9b03324

31. Zhou J, Xu N-S, Deng S-Z, Chen J, She J-C, Wang Z-L (2003) Large-area nanowire arrays of molybdenum and molybdenum oxides: synthesis and field emission properties. Adv Mater 15(21):1835–1840. https://doi.org/10.1002/adma.200305528

32. Shon JK, Lee HS, Park GO, Yoon J, Park E, Park GS, Kong SS, Jin M, Choi J-M, Chang H, Doo S, Kim JM, Yoon W-S, Pak C, Kim H, Stucky GD (2016) Discovery of abnormal lithium-storage sites in molybdenum dioxide electrodes. Nat Commun 7(1):11049. https://doi.org/10.1038/ncomms11049

33. Itika K, Babu GVR, Jayesh TB, Rao KSR, Nagaraja BM (2017) Synchronized dehydrogenation-hydrogenation reactions over partially reduced MoO2 based catalyst for simultaneous synthesis of styrene and aniline. Catal Commun 90:27–30. https://doi.org/10.1016/j.catcom.2016.11.013

34. Sun Y, Hu X, Yu JC, Li Q, Luo W, Yuan L, Zhang W, Huang Y (2011) Morphosynthesis of a hierarchical MoO2 nanoarchitecture as a binder-free anode for lithium-ion batteries. Energy Environ Sci 4(8):2870–2877. https://doi.org/10.1039/C1EE01189H

35. Luo W, Hu X, Sun Y, Huang Y (2011) Electrospinning of carbon-coated MoO2 nanofibers with enhanced lithium-storage properties. Phys Chem Chem Phys 13(37):16735–16740. https://doi.org/10.1039/C1CP22184A

36. Bento A, Sanches A, Medina E, Nunes CD, Vaz PD (2015) MoO2 nanoparticles as highly efficient olefin epoxidation catalysts. Appl Catal A Gen 504:399–407. https://doi.org/10.1016/j.apcata.2015.03.024

37. Ni J, Zhao Y, Li L, Mai L (2015) Ultrathin MoO2 nanosheets for superior lithium storage. Nano Energy 11:129–135. https://doi.org/10.1016/j.nanoen.2014.10.027

38. Qing M, Meng Y, Wang Y, Li X, Zhou C, Liang Y, Zhang Z, Liu Q, Guo Y, Xiao D (2019) Building nanoparticle-stacking MoO2-CDs via in-situ carbon dots reduction as high-performance anode material for lithium ion and sodium

Wazir *et al. Nanoscale Research Letters* (2020) 15:156

Page 9 of 9

ion batteries. Electrochim Acta 319:740–752. https://doi.org/10.1016/j.electacta.2019.07.017

39. Razaq R, Sun D, Xin Y, Li Q, Huang T, Zhang Z, Huang Y (2019) Nanoparticle assembled mesoporous MoO2 microrods derived from metal organic framework and wrapped with graphene as the sulfur host for long-life lithium–sulfur batteries. Adv Mater Interfaces 6(4):1801636. https://doi.org/10.1002/admi.201801636

40. Lee E, Yoon YS, Kim D-J (2018) Two-dimensional transition metal dichalcogenides and metal oxide hybrids for gas sensing. ACS Sensors 3(10):2045–2060. https://doi.org/10.1021/acssensors.8b01077

41. Domínguez A, Dutt A, de Melo O, Huerta L, Santana G (2018) Molybdenum oxide 2-D flakes: role of thickness and annealing treatment on the optoelectronic properties of the material. J Mater Sci 53(8):6147–6156. https://doi.org/10.1007/s10853-017-1975-8

42. Inzani K, Nematollahi M, Vullum-Bruer F, Grande T, Reenaas TW, Selbach SM (2017) Electronic properties of reduced molybdenum oxides. Phys Chem Chem Phys 19(13):9232–9245. https://doi.org/10.1039/C7CP00644F

43. Itikawa Y (2007) Molecular processes in plasmas: collisions of charged particles with molecules. molecular processes in plasmas: collisions of charged particles with molecules

44. Ya C, Wang B (2019) Effects of deposition parameters on structures and photoluminescence of MoO3-x nanomaterials grown by CVD. Opt Mater 92: 150–155. https://doi.org/10.1016/j.optmat.2019.04.010

45. Wang BB, Qu XL, Zhu MK, Chen YA, Zheng K, Zhong XX, Cvelbar U, Ostrikov K (2018) Plasma produced photoluminescent molybdenum sub-oxide nanophase materials. J Alloys Compd 765:1167–1173. https://doi.org/10.1016/j.jallcom.2018.06.279

46. Lalik E, David WIF, Barnes P, Turner JFC (2001) Mechanisms of reduction of MoO3 to MoO2 reconciled? J Phys Chem B 105(38):9153–9156. https://doi.org/10.1021/jp011622p

47. Kumar V, Sumboja A, Wang J, Bhavanasi V, Nguyen VC, Lee PS (2014) Topotactic phase transformation of hexagonal MoO3 to layered MoO3-II and its two-dimensional (2D) nanosheets. Chem Mater 26(19):5533–5539. https://doi.org/10.1021/cm502558t

48. Zheng L, Xu Y, Jin D, Xie Y (2009) Novel Metastable Hexagonal MoO3 Nanobelts: Synthesis, Photochromic, and Electrochromic Properties. Chem Mater 21(23):5681–5690. https://doi.org/10.1021/cm9023887

49. Xu X, Li X, Liu K, Li J, Feng Q, Zhou L, Cui F, Liang X, Lei Z, Liu Z, Xu H (2018) Thermodynamics and kinetics synergetic phase-engineering of chemical vapor deposition grown single crystal MoTe2 nanosheets. Cryst Growth Des 18(5):2844–2850. https://doi.org/10.1021/acs.cgd.7b01624

50. Wang S, Rong Y, Fan Y, Pacios M, Bhaskaran H, He K, Warner JH (2014) Shape evolution of monolayer MoS2 crystals grown by chemical vapor deposition. Chem Mater 26(22):6371–6379. https://doi.org/10.1021/cm5025662

51. Yang X, Wang Y, Zhou J, Liu Z (2017) Temperature-dependent morphology of chemical vapor grown molybdenum disulfide. J Phys D Appl Phys 50(16): 164002. https://doi.org/10.1088/1361-6463/aa6220

52. Frisenda R, Island JO, Lado JL, Giovanelli E, Gant P, Nagler P, Bange S, Lupton JM, Schüller C, Molina-Mendoza AJ, Aballe L, Foerster M, Korn T, Angel Niño M, de Lara DP, Pérez EM, Fernandéz-Rossier J, Castellanos-Gomez A (2017) Characterization of highly crystalline lead iodide nanosheets prepared by room-temperature solution processing. Nanotechnology 28(45):455703. https://doi.org/10.1088/1361-6528/aa8e5c

53. Kalantar-zadeh K, Tang J, Wang M, Wang KL, Shailos A, Galatsis K, Kojima R, Strong V, Lech A, Wlodarski W, Kaner RB (2010) Synthesis of nanometre-thick MoO3 sheets. Nanoscale 2(3):429–433. https://doi.org/10.1039/B9NR00320G

54. Pu E, Liu D, Ren P, Zhou W, Tang D, Xiang B, Wang Y, Miao J (2017) Ultrathin MoO2 nanosheets with good thermal stability and high conductivity. AIP Adv 7(2):025015. https://doi.org/10.1063/1.4977543

55. Vorobeva NS, Lipatov A, Muratov DS, Sinitskii A (2018) Chemical vapor deposition and characterization of two-dimensional molybdenum dioxide (MoO2) nanoplatelets. Nanotechnology 29(50):505707. https://doi.org/10.1088/1361-6528/aae366

56. Wang D, Li J-N, Zhou Y, Xu D-H, Xiong X, Peng R-W, Wang M (2016) Van der Waals epitaxy of ultrathin α-MoO3 sheets on mica substrate with single-unit-cell thickness. Appl Phys Lett 108(5). https://doi.org/10.1063/1.4941402

57. Liu H, Cai Y, Han M, Guo S, Lin M, Zhao M, Zhang Y, Chi D (2018) Aqueous and mechanical exfoliation, unique properties, and theoretical understanding of MoO3 nanosheets made from free-standing α-MoO3

crystals: Raman mode softening and absorption edge blue shift. Nano Res 11(3):1193–1203. https://doi.org/10.1007/s12274-017-1733-x

58. Mestl G, Ruiz P, Delmon B, Knozinger H (1994) Oxygen-Exchange Properties of MoO3: An in situ Raman Spectroscopy Study. J Phys Chem 98(44):11269–11275. https://doi.org/10.1021/j100095a007

59. Klinbumrung A, Thongtem T, Thongtem S (2012) Characterization of orthorhombic α-MoO microplates produced by a microwave plasma process. J Nanomater 2012:5. https://doi.org/10.1155/2012/930763

60. Dieterle M, Mestl G (2002) Raman spectroscopy of molybdenum oxides Part II. Resonance Raman spectroscopic characterization of the molybdenum oxides Mo4O11 and MoO2. Phys Chem Chem Phys 4(5):822–826. https://doi.org/10.1039/B107046K

61. Wu D, Yang Y, Zhu P, Zheng X, Chen X, Shi J, Song F, Gao X, Zhang X, Ouyang F, Xiong X, Gao Y, Huang H (2018) Epitaxial growth of highly oriented metallic MoO2@MoS2 nanorods on C-sapphire. J Phys Chem C 122(3):1860–1866. https://doi.org/10.1021/acs.jpcc.7b10666

62. Alsaif MMYA, Chrimes AF, Daeneke T, Balendhran S, Bellisario DO, Son Y, Field MR, Zhang W, Nili H, Nguyen EP, Latham K, van Embden J, Strano MS, Ou JZ, Kalantar-zadeh K (2016) High-performance field effect transistors using electronic inks of 2D molybdenum oxide nanoflakes. Adv Funct Mater 26(1):91–100. https://doi.org/10.1002/adfm.201503698

63. Alsaif MMYA, Latham K, Field MR, Yao DD, Medehkar NV, Beane GA, Kaner RB, Russo SP, Ou JZ, Kalantar-zadeh K (2014) Tunable plasmon resonances in two-dimensional molybdenum oxide nanoflakes. Adv Mater 26(23):3931–3937. https://doi.org/10.1002/adma.201306097

64. Navas I, Vinodkumar R, Mahadevan Pillai VP (2011) Self-assembly and photoluminescence of molybdenum oxide nanoparticles. Applied Physics A 103(2):373. https://doi.org/10.1007/s00339-011-6345-9

65. Díaz-Guerra C, Chioncel MF, Piqueras J (2009) Structural and cathodoluminescence assessment of transition metal oxide nanostructures grown by thermal deposition methods. Superlattice Microst 45(4):145–150. https://doi.org/10.1016/j.spmi.2008.11.014

66. Pierret A, Loayza J, Berini B, Betz A, Plaçais B, Ducastelle F, Barjon J, Loiseau A (2014) Excitonic recombinations in h-BN: From bulk to exfoliated layers. Phys Rev B 89:035414

67. Bourrellier R, Meuret S, Tararan A, Stéphan O, Kociak M, Tizei LHG, Zobelli A (2016) Bright UV single photon emission at point defects in h-BN. Nano Lett 16(7):4317–4321. https://doi.org/10.1021/acs.nanolett.6b01368

68. Zhou N, Gan L, Yang R, Wang F, Li L, Chen Y, Li D, Zhai T (2019) Nonlayered two-dimensional defective semiconductor γ-Ga2S3 toward broadband photodetection. ACS Nano 13(6):6297–6307. https://doi.org/10.1021/acsnano.9b00276

Publisher's Note